Acta Crystallographica Section D
Biological Crystallography
ISSN 0907-4449

Structure of hydroxynitrile lyase from *Manihot esculenta* in complex with substrates acetone and chloroacetone: implications for the mechanism of cyanogenesis

Hanspeter Lauble,[a]* Siegfried Förster,[a] Burkhard Miehlich,[a] Harald Wajant[b] and Franz Effenberger[a]

[a]Universität Stuttgart, Institut für Organische Chemie, Pfaffenwaldring 55, D-70569 Stuttgart, Germany, and [b]Universität Stuttgart, Institut für Zellbiologie und Immunologie, D-70569 Stuttgart, Germany

Correspondence e-mail: peterlauble@t-online.de

Received 6 July 2000
Accepted 31 October 2000

PDB References: MeHNL–acetone complex, 1dwo; MeHNL–chloroacetone complex, 1dwq.

The crystal structures of hydroxynitrile lyase from *Manihot esculenta* (MeHNL) complexed with the native substrate acetone and substrate analogue chloroacetone have been determined and refined at 2.2 Å resolution. The substrates are positioned in the active site by hydrogen-bond interactions of the carbonyl O atom with Thr11 OG, Ser80 OG and, to a lesser extent, Cys81 SG. These studies support a mechanism for cyanogenesis as well as for the stereospecific MeHNL-catalyzed formation of (*S*)-cyanohydrins, which closely resembles the base-catalyzed chemical reaction of HCN with carbonyl compounds.

1. Introduction

Hydroxynitrile lyases catalyze the decomposition of a variety of cyanohydrins into their corresponding carbonyl compounds and HCN. The release of toxic HCN by these enzymes is believed to play a central role in the defence mechanism of plants against herbivores (Seigler, 1991). Numerous reports dealing with the isolation, purification, characterization and substrate specificities of HNLs from various species have been published (Wajant & Effenberger, 1996). The enzymes appear to fall into several groups which can be distinguished according to sequence homology and biochemical properties such as subunit composition, cofactor requirement and the stereospecificity of enzymatic reaction (Gerstner & Pfeil, 1972; Hasslacher *et al.*, 1996; Wajant & Effenberger, 1996; Wajant & Pfizenmaier, 1996; Trummler & Wajant, 1997). Consequently, it is supposed that HNLs have evolved independently several times from various distinct ancestral molecules (Wajant *et al.*, 1994; Trummler & Wajant, 1997). Apart from the interesting aspects of the molecular evolution of the catalytic function, HNLs are of importance as biocatalysts in organic chemistry for preparations of optically active cyanohydrins with high optical yields (North, 1993; Effenberger, 1994, 1999; Förster *et al.*, 1996; Schmidt *et al.*, 1996; Griengl *et al.*, 1997).

Two mechanisms have been proposed for the reaction catalyzed by HNLs. One mechanism, based on the crystal structure of *Hevea brasiliensis* (HbHNL) in complex with histidine, involves addition of acetone cyanohydrin to HbHNL to form a tetrahedral hemiketal intermediate followed by elimination of HCN (Wagner *et al.*, 1996). The second mechanism, originally postulated by Wajant & Pfizenmaier (1996), closely resembles the base-catalyzed chemical reaction of HCN with carbonyl compounds. Experimental evidence supporting this general base mechanism is provided from the crystal structure of the HbHNL–acetone complex (Zuegg *et al.*, 1999). Although the structure of the HbHNL–acetone

complex represents the binding mode with the native substrate, it is difficult to assert the validity of one of the two proposed catalytic mechanisms unambiguously, as the acetone-soaking experiment of HbHNL was performed at pH 7.5, a pH range outside the pH optimum (Wajant & Förster, 1996).

In the present publication, we report the refined 2.2 Å structures of MeHNL in complexes with the substrates acetone and chloroacetone, respectively. Soaking experiments were performed under physiological pH conditions (pH 5.4), corresponding to the maximum of enzymatic activity. With these structures we can define the residues that are important for cyanogenesis and also give an explanation for the stereoselectivity of the enzyme-catalyzed cyanohydrin formation.

2. Materials and methods

2.1. Materials

Recombinant MeHNL was overexpressed and purified as described elsewhere (Förster *et al.*, 1996). All chemicals used were purchased from Sigma.

2.2. Crystallization and X-ray crystallographic data collection

Crystallization of MeHNL was performed as reported previously (Lauble *et al.*, 1999). Acetone-complexed MeHNL crystals were obtained by soaking the native MeHNL crystals (0.7 × 0.8 × 0.7 mm) in a stabilization buffer containing 100 m*M* sodium citrate pH 5.4, 6% poly(ethylene glycol) 8000 (PEG 8000), 28% 2-methyl-2,4-pentanediol (MPD) and a stepwise increasing acetone concentration of 10, 50, 200, 500 m*M*, 1.5 and 3.0 *M*. Soaking in a significantly increased concentration of acetone was performed to compensate for the low binding activity of the native substrate (Wajant & Pfizenmaier, 1996; Wajant & Förster, 1996). The crystals were flash-cooled at 100 K after a total soaking time of 1 h. These acetone-complexed MeHNL crystals belong to the tetragonal space group $P4_12_12$, with unit-cell parameters a = 105.5, c = 188.5 Å.

Chloroacetone-complexed crystals were obtained following the soaking protocol described above. Native MeHNL crystals were transferred into a stabilization buffer containing 100 m*M* sodium citrate pH 5.4, 6% PEG 8000, 28% MPD and a stepwise increasing chloroacetone concentration of 5, 10, 50, 300 and 800 m*M*. One crystal was flash-cooled at 100 K after a total soaking time of 30 min. The chloroacetone-complexed MeHNL crystals are isomorphous to the acetone-complexed crystals, with unit-cell parameters a = 105.9, c = 188.4 Å.

Synchrotron X-ray data were collected from one crystal at 100 K on beamline X11 of the EMBL outstation in Hamburg at a wavelength of 0.902 Å using a MAR Research image-plate detector system. Data were indexed and integrated using *DENZO* (Otwinowski, 1993) and scaled and reduced with the *CCP*4 suite of programs (Collaborative Computational Project, Number 4, 1994). Data-collection statistics are given in Table 1.

Table 1
Data-collection statistics.

Values in parentheses refer to the outer shell, 2.30–2.20 Å.

Model	MeHNL–acetone	MeHNL–chloroacetone
Space group	$P4_12_12$	$P4_12_12$
Unit-cell parameters (Å)	$a = b$ = 105.5, c = 188.5	$a = b$ = 105.9, c = 188.4
Maximum resolution (Å)	2.10	2.10
Resolution of data collection (Å)	15.0–2.20	20.0–2.20
No. of observations	215742	207542
Unique reflections	52853	54130
Mosaicity (°)	0.2	0.2
Completeness (%)	97.1 (99.4)	96.7 (98.2)
Average multiplicity	4.2 (4.1)	3.8 (3.8)
$I/\sigma(I)$	8.6 (3.2)	7.5 (3.1)
R_{sym}† (%)	6.8 (14.1)	7.4 (15.9)

† $R_{sym} = \sum_{hkl}\sum_i |I_i - \langle I\rangle| / \sum_i I_i$, where I_i is the intensity of the ith reflection (hkl) or a symmetry-related reflection and $\langle I\rangle$ is the scaled mean intensity. The summation is over all measured reflections.

2.3. Refinement of the MeHNL–acetone complex

The starting model for refinement of the MeHNL–acetone complex was the 2.2 Å resolution refined MeHNL–acetate structure (PDB entry 1dwp) with water molecules and acetate deleted. This crystal contains two molecules in the crystallographic asymmetric unit, while MeHNL is reported to exist as a tetramer in solution (Wajant *et al.*, 1995; Chueskul & Chulavatnatol, 1996). Molecule *A* consists of 262 amino acids and molecule *B* 258 amino acids. The extra four residues Pro, Ile, Ser and Lys of molecule *A* are part of the seven residues encoded by the multiple cloning site of the expression vector (Wajant & Pfizenmaier, 1996) used for overexpression of MeHNL. This amino-terminal modification is in agreement with biochemical experiments showing that the amino-terminus of MeHNL is not fully accessible by classical Edman degradation (data not shown). Owing to the slight change in unit-cell parameters, the dimer comprising the asymmetric unit was subjected to a rigid-body refinement allowing the rearrangement of both molecules against each other. Conventional coordinate refinement using simulated annealing with *X-PLOR* (Brünger, 1992*a*,*b*) resulted in a model with R_{cryst} = 26.5% and R_{free} = 29.3% for all data in the resolution range 8–2.5 Å. $2|F_o| - |F_c|$ and $|F_o| - |F_c|$ difference Fourier maps were calculated and carefully inspected on an IRIS workstation using the program *FRODO* (Jones, 1978). Water molecules were added using the solvent structure of the MeHNL–acetate complex (PDB entry 1dwp) as a guideline. Subsequent positional and *B*-factor refinement converged to R_{cryst} = 21.3% and R_{free} = 26.5% for 45 239 reflections in the resolution range 8–2.3 Å. Electron-density maps calculated with coefficients $2|F_o| - |F_c|$ and $|F_o| - |F_c|$ clearly showed that acetone was bound by the enzyme at the active site of subunit *A*. The carbonyl O atom of acetone was placed into the density in such a way as to produce the most favoured hydrogen-bond contacts. The model presented here is also compatible with the substrate orientation in the chloroacetone complex, where the Cl atom permits an unambiguous assignment of the substrate orientation. The binding pocket of subunit *B* has rather weak

Table 2
Refinement statistics and stereochemical quality of the final models.

$R = 100\sum_{hkl}|F_{(\mathrm{obs},\,hkl)} - F_{(\mathrm{calc},\,hkl)}|/\sum_{h}F_{(\mathrm{obs},\,hkl)}$, where $F_{(\mathrm{obs})}$ and $F_{(\mathrm{calc})}$ are the observed and calculated structure-factor amplitudes, respectively, and the summation is over all reflections *hkl*. R_{cryst} and R_{free} are calculated using the working and free reflection sets, respectively.

Model	MeHNL–acetone	MeHNL–chloroacetone
No. protein non-H atoms	4178	4186
No. of water molecules	273	211
No. of acetone atoms	4	—
No. of chloroacetone atoms	—	5
Resolution range (Å)	8.0–2.2	8.0–2.2
No. of reflections ($F_o > 2\sigma F_o$)	51240	51410
No. of reflections for R_{free} ($F_o > 2\sigma F_o$)	5303	5419
R_{cryst} (%)	19.2	20.7
R_{free} (%)	25.2	24.4
R.m.s. deviation from target values		
Bond lengths (Å)	0.009	0.010
Bond angles (°)	2.1	2.9
Dihedrals (°)	21.2	23.6
ΔB, bonded atoms (Å^2)	2.9	3.2
Ramachandran plot (%)		
Most favoured region	89.0	87.0
Additionally allowed region	9.7	11.7
Generously allowed region	0.4	0.4
Disallowed region	0.9	0.9
Average *B* factors		
Protein (Å^2)	19	28
Waters (Å^2)	31	39
Acetone (Å^2)	27	—
Chloroacetone (Å^2)	—	39

density that could not be attributed to acetone and has therefore been modelled as two water molecules. All residues surrounding the active-site pocket of molecule *B*, however, remain well defined and do not display high *B* factors. The protein structure with the water molecules and the fitted model of acetone was refined against data in the resolution range 8–2.2 Å. Appropriate restraints for acetone were incorporated in the *X-PLOR* directory on the basis of the small-molecule structure generated by *INSIGHT II*/*DISCOVER* (BIOSYM/Molecular Simulations Inc., 1995). The final $|F_o| - |F_c|$ difference Fourier map showed no significant residual features. Refinement statistics are summarized in Table 2.

2.4. Refinement of the MeHNL–chloroacetone complex

The unit-cell parameters of the MeHNL–chloroacetone complex crystals are similar to those of the acetone complex and the previously refined structure was therefore used as a starting model, but without substrate and without water molecules close to the active sites. A rigid-body refinement was performed followed by positional refinement. Simulated annealing with *X-PLOR* (Brünger, 1992*a*,*b*) resulted in a model with R_{cryst} = 24.4% and R_{free} = 29.0% for all data in the resolution range 8–2.4 Å. $2|F_o| - |F_c|$ and $|F_o| - |F_c|$ Fourier maps were calculated and water molecules were corrected if necessary. Subsequent positional and *B*-factor refinement converged to *R* factors of R_{cryst} = 21.2%, R_{free} = 25.8% for 51 410 reflections in the resolution range 8–2.2 Å.

At 2.2 Å resolution, the electron density corresponding to chloroacetone was unambiguously interpretable in $2|F_o| - |F_c|$ and $|F_o| - |F_c|$ Fourier maps, although only in the active site of molecule *A*. The electron density found in the vicinity of the active-site *B* residues Ser80 and His236 is weak and rather diffuse and was therefore modelled as two water molecules. For chloroacetone refinement the structure of the substrate was defined with freely varying torsion angles, but with bond lengths, angles and trigonal atom planarity defined from its *INSIGHT II*/*DISCOVER* structure. Extra electron density was found in both subunits at the side chain of Cys81. Owing to the alkylation potential of chloroacetone and because the extraneous electron density was large enough to accommodate a four-atom group, it was modelled as an acetonyl ($CH_3-CO-CH_2$) moiety. Subsequent positional and *B*-factor refinement of the protein structure with the water molecules, the fitted model of chloroacetone and the modified Cys81 residues converged to R_{cryst} = 20.7% and R_{free} = 24.4% in the resolution range 8–2.2 Å. The final $|F_o| - |F_c|$ difference Fourier map showed no significant residual features. Refinement statistics are summarized in Table 2.

3. Results and discussion

3.1. MeHNL complex with acetone

The refined structure of the MeHNL–acetone complex consists of 4178 non-H protein atoms containing all 520 residues of both molecules in the asymmetric unit, one acetone molecule and a total of 273 water molecules (Table 2). The refinement of the final model converged to R_{cryst} = 19.2%, R_{free} = 25.2% for 51 240 reflections in the resolution range 8–2.2 Å. In the Ramachandran plot, 89.0% of the residues are in the most favoured region and 9.7% are in the additionally allowed parts (Table 2). Two residues, Ser80 and Arg129, are outside the allowed regions for both molecules *A* and *B*. The active-site residue Ser80 has well defined electron density and Arg129 has high-energy main-chain torsion angles owing to a salt-bridge contact to Glu156. A comparison of the two independently refined molecules in the asymmetric unit shows r.m.s. differences of 0.4 Å for all protein atoms. The tertiary fold of the acetone-complexed MeHNL structure is also very

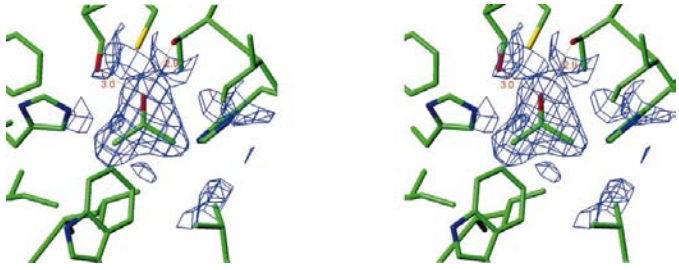

Figure 1
Stereoview of $2|F_o| - |F_c|$ simulated-annealing map (15–2.2 Å) of the acetone complex contoured at 1σ, showing the density of the substrate between His236 and Ser80. The distance from the scissile carbonyl O atom to the catalytic Ser80 OG is 3.0 Å.

similar to the HbHNL–acetone complex (Zuegg *et al.*, 1999), with an r.m.s. deviation for the 253 common C^{α} atoms of 0.42 Å. The largest differences between the two molecules occur on the surface, while the active-site residues superimpose very well with an r.m.s. of 0.23 Å for all atoms.

The active site of MeHNL is located in a cavity buried inside the enzyme and is only accessible to solvent *via* a narrow tunnel. The trigonal planar shape of the electron density in the active site of molecule *A* (Fig. 1) clearly shows that acetone was bound by the enzyme at a single site with high occupancy. The ambiguity in defining the detailed orientation of the methyl group and the carbonyl O atom in the observed electron density has been solved by using chloroacetone as reference (see below).

The molecular basis of binding the carbonyl substrates as observed in MeHNL is shown in Fig. 2. The acetone carbonyl O atom is hydrogen bonded to (i) Thr11 OG (2.9 Å), (ii) Ser80 OG (3.0 Å) and, to a lesser extent, (iii) Cys81 SG (3.3 Å).

The model presented here is in agreement with site-directed mutagenesis experiments showing that Ser80 is absolutely essential for catalytic activity (Wajant & Pfizenmaier, 1996), while Thr11 seems to be involved in substrate binding and proper orientation. One methyl group of acetone (labelled C1) is held in position by van der Waals contacts to Leu149 CD1 (3.7 Å), Thr11 CG2 (4.1 Å) and Ile12 CG1 (4.0 Å). The side chains of these three residues define a small hydrophobic specificity site S_1 near the catalytic site. In contrast, the second methyl group (labelled C3) points into the opposite direction towards the active-site tunnel, defining the putative second subsite S_2 in the binding cavity. The C3 atom is in van der Waals contact with Ile210 CD1 (3.8 Å), Trp128 CZ3 (4.0 Å) and Leu158 CD2 (4.3 Å) (Fig. 2). Only one water molecule was located and verified near the binding pocket of molecule *A*; however, it is not in direct contact with the side chain of a catalytic residue. Despite working with saturating acetone concentration under physiological pH conditions, only molecule *A* of the asymmetric unit shows unambiguously clear electron density. The rather diffuse density found in molecule *B* was modelled as two water molecules. The finding that the active sites of the two MeHNL molecules comprising the asymmetric unit bind substrate in an unsymmetrical manner becomes understandable in view of the different crystal packing contacts in which the two molecules are involved. While the entrance to the active site of molecule *A* is oriented towards a large empty solvent channel, the entrance to the active site of molecule *B* is packed in the crystal lattice towards a small solvent channel created by atoms of a symmetry-related molecule, making the entrance to the binding pocket of subunit *B* less accessible towards the substrate. Important for this study is that similar features are observed in both the MeHNL–acetone and MeHNL–chloroacetone structures.

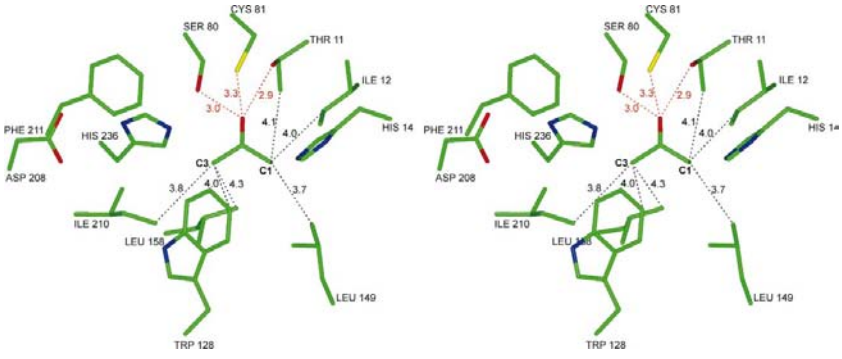

Figure 2
Stereoview showing the intermolecular interactions between acetone and selected active-site residues. Hydrogen bonds are shown as red dashed lines and van der Waals interactions as black dashed lines.

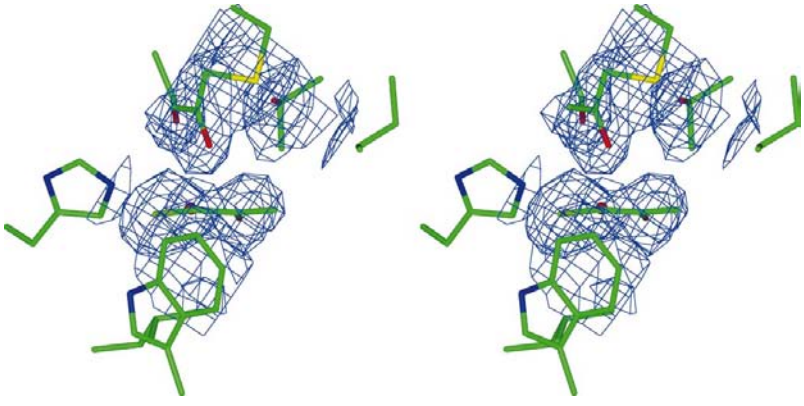

Figure 3
Stereoview of $2|F_o| - |F_c|$ map (20–2.2 Å) of the chloroacetone complex contoured at 1σ. On top of the map, the density for the alkylated Cys81 side chain is visible.

3.2. MeHNL complex with chloroacetone

The refined structure of the MeHNL–chloroacetone complex consists of 4186 non-H protein atoms containing 520 residues of both molecules in the asymmetric unit, one chloroacetone molecule and 211 water molecules (Table 2). The model included SG of Cys81 of each monomer as an acetonyl moiety based on electron density (see §2; Fig. 3). The *R* factors for the final model are $R_{\rm cryst} = 20.7\%$ and $R_{\rm free} = 24.4\%$ for all 51 410 reflections in the resolution range 8–2.2 Å (Table 2). Superposition of the two independently refined molecules in the asymmetric unit shows r.m.s. differences of 0.45 Å for all atoms.

The chloroacetone molecule is well defined in the electron-density map, as the Cl atom results in an unambiguous electron-density peak (Fig. 3).

The interactions of chloroacetone at the MeHNL active site are similar to those of acetone in the MeHNL–acetone complex structure, although with some positional shifts. The carbonyl O atom is hydrogen bonded to the active-site cavity water molecule W16

Table 3
Preparation of (*S*)-ketone cyanohydrins by MeHNL-catalyzed addition of HCN to aliphatic methyl and ethyl ketones.

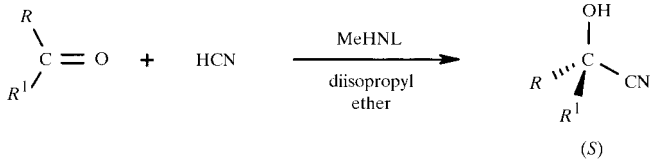

ee, enantiomeric excess.

Substrate					
	R	R^1	Time (h)	Yield (%)	ee (%)
2-butanone	C_2H_5	CH_3	4.0	91	18
2-pentanone	C_3H_7	CH_3	0.5	36	69
2-hexanone	C_4H_9	CH_3	0.5	58	80
2-heptanone	C_5H_{11}	CH_3	2.0	39	92
3-heptanone	C_4H_9	C_2H_5	5.0	40	45
3-octanone	C_5H_{11}	C_2H_5	6.0	24	61

(2.7 Å) and shows weak interactions with Ser80 OG (3.7 Å) and Thr11 OG1 (3.9 Å). The methyl group (labelled C1) points into the apolar binding cavity S_1, making van der Waals contacts with (i) Ile12 CG1 (3.4 Å), (ii) Ile12 CD1 (4.0 Å) and (iii) Trp128 CZ3 (4.0 Å). The methyl group C1 shows also an interaction with the alkylated Cys81 O4 (3.5 Å). The methylene group (labelled C3) interacts with Cys81 O4 (3.0 Å) and Ser80 OG (3.4 Å) and is in contact with the S_2 binding site *via* van der Waals interactions with Trp128 CH2 (3.8 Å) and Trp128 CZ3 (3.9 Å). The most important interactions of the Cl atom include (i) Ser80 OG (3.1 Å), (ii) active-site water W16 (3.1 Å), (iii) His236 NE2 (3.3 Å), (iv) Ile210 CD1 (3.7 Å), (v) Phe211 CE1 (3.7 Å) and (vi) Leu158 CG (4.0 Å). The hydrogen bonding and van der Waals interactions of chloroacetone are further highlighted in Fig. 4.

As in the MeHNL–acetone complex structure, there is only density for the substrate at the active site of molecule *A*, which is consistent with our interpretation that the active site of molecule *B* is not accessible to the soaking component owing to crystal lattice contacts.

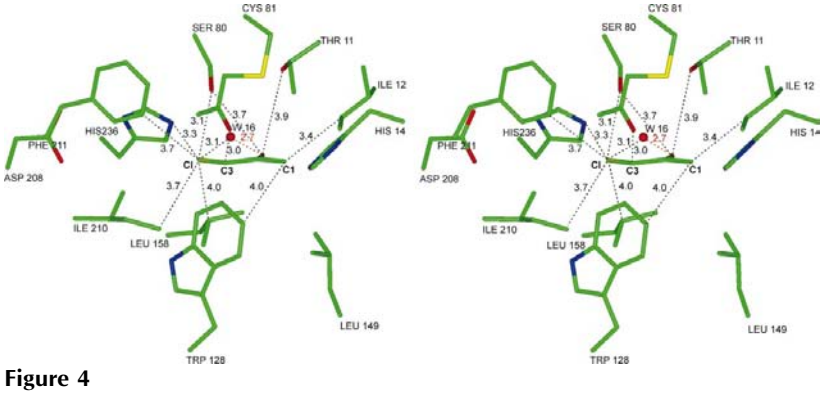

Figure 4
Stereoview showing the intermolecular interactions between chloroacetone and selected active-site residues. Hydrogen bonds are shown as red dashed lines and van der Waals interactions as black dashed lines.

Least-squares superpositioning of the MeHNL–acetone complex and the MeHNL–chloroacetone complex structure shows r.m.s. deviation of 0.19 Å for all atoms of the active-site residues and 0.20 Å for the polypeptide backbone atoms. Notwithstanding the similarities in the structures of the two complex models, there are some differences. In the MeHNL–chloroacetone complex, the chloroacetone is displaced from the acetone-binding position by 1.0 Å and the carbonyl O atom is 3.7 Å away from Ser80 OG compared with 3.0 Å in the MeHNL–acetone structure. This difference in substrate orientation is possibly caused by the alkylation of Cys81, rather than the use of the substrate analogue. Superposition of acetone onto the corresponding atomic positions in the MeHNL–chloroacetone complex shows that any binding of a ketone into an alkylated Cys81 active site must lead to a different orientation to avoid a steric conflict between the carbonyl O atom and the alkylated side chain of Cys81.

3.3. Substrate specificity of MeHNL-catalyzed cyanohydrin formation

For the reverse reaction of cyanogenesis, *i.e.* the conversion of carbonyl compounds to cyanohydrins, the stereochemistry and the substrate specificity have been studied intensively (Förster *et al.*, 1996). The wild-type enzyme was characterized with respect to the enantiomeric excess (ee) of the corresponding cyanohydrin using a series of aliphatic ketones as input substrates (Förster *et al.*, 1996) (Table 3).

As can be seen from Table 3, the stereoselectivity of the reaction is (*S*) towards prochiral ketones and the enantioselectivity clearly depends on the length of substituents *R*. The pronounced asymmetric architecture of the small S_1 site and the large S_2 binding pocket seems to be a dominant factor for the substrate specificity. 2-Butanone has small *R* and R^1 substituents and these groups are easily accommodated in the binding pockets in a way that *R* is placed either into the S_2 site or alternatively into the S_1 site. A consequence of these two possible binding modes is the low enantiomeric excess of 18% for the cyanohydrin (Table 3). Replacement of $R = C_2H_5$ by C_3H_7 increases the enantioselectivity for the cyanohydrin formation (Table 3), suggesting that 2-pentanone prefers to bind in a mode where the larger C_3H_7 group points towards the S_2 pocket, while the smaller CH_3 group is placed into the S_1 site. Model building shows that the binding of propyl ($R^1 = C_3H_7$) in a similar way into the smaller S_1 site brings the propyl moiety into close contact with the main-chain and side-chain atoms of Leu149 and Leu158, respectively, and would therefore be more unfavourable. When *R* is substituted with C_4H_9 and larger alkyl groups ($R = C_5H_{11}$), respectively, there is a significant increase in enantioselectivity. The restricted volume of the small S_1 cavity does not allow the accommodation of the C_4H_9 moiety, while such a bulky group is easily accommodated in the larger S_2 pocket.

3.4. Implications for the mechanism of cyanogenesis

To date, only one X-ray crystallographic structure of HNL–substrate complexes, the HbHNL–acetone complex, has been reported (Zuegg *et al.*, 1999). The results described in the present publication for MeHNL structure complexed with acetone and chloroacetone were compared with the previous findings. The HbHNL and MeHNL enzymes show 75% sequence identity and the crystal structures of the acetone complexes superimpose with an r.m.s. deviation of 0.42 Å for the 253 common C^{α} atoms and with an r.m.s. deviation of 0.23 Å for all atoms of the active-site residues. The similarity of the substrate binding in both the MeHNL–acetone and HbHNL–acetone complex is also very clear. Although the binding mode for acetone found in the two HNLs is basically identical, the MeHNL binding subsite is distinct from the HbHNL subsite in the following way: in the HbHNL–acetone complex a water molecule is located between His235 and Lys236 (HbHNL numbering). According to Zuegg *et al.* (1999), the HbHNL–acetone active-site water molecule is replaced by incoming cyanide which is then stabilized by interaction with His235 and Lys236 (HbHNL numbering). In the MeHNL–acetone structure no water molecule is located at the corresponding position in the binding pocket of molecule *A*.

Differences in the hydration mode of two crystal structures may be caused by different crystallization conditions and it should be noted therefore that the MeHNL was crystallized at the physiological pH 5.4, corresponding to the maximum of enzyme activity, using a mixture of PEG 8000 and MPD as precipitant, while HbHNL was crystallized at pH 7.5, a non-optimum, using PEG 400 and $(NH_4)_2SO_4$ as precipitants (Zuegg *et al.*, 1999). Furthermore, the acetone complex observed for HbHNL was obtained by soaking the crystal with 400 m*M* acetone (Zuegg *et al.*, 1999), while the MeHNL–acetone complex structure was obtained by soaking performed with 3 *M* acetone (see §2.2). The high substrate concentration was chosen to compensate for the low acetone-binding affinity to HNL, reflected by a K_m of 120 m*M* (Wajant & Pfizenmaier, 1996). The possibility that the acetone-binding mode observed for MeHNL represents an unproductive complex is therefore unlikely.

Fig. 5 summarizes our conclusions concerning the catalytic mechanism of MeHNL. As shown, the ketone carbonyl O atom is hydrogen bonded to Ser80 OG and Thr11 OG. The optimal hydrogen-bond geometry also activates the substrate through polarization of the carbonyl, rendering the carbonyl C atom of ketones highly susceptible to nucleophilic attack. This binding mode suggests that the incoming nucleophile cyanide exclusively attacks the *Si* face of the carbonyl group when bound to the active site of the enzyme (Fig. 2), implying that the deprotonation of hydrogen cyanide has to be performed by His236 which is located on the *Si* face of the carbonyl compound in order to be consistent with the (*S*)-stereospecificity of the addition. Addition of cyanide to the carbonyl group, proton transfer from Ser80 to the carbonyl O atom and proton transfer from His236 to Ser80 forming the (*S*)-cyanohydrin then occur simultaneously (Fig. 5). The last step of catalytic cycle is the release of the cyanohydrin and reconstitution of the active site.

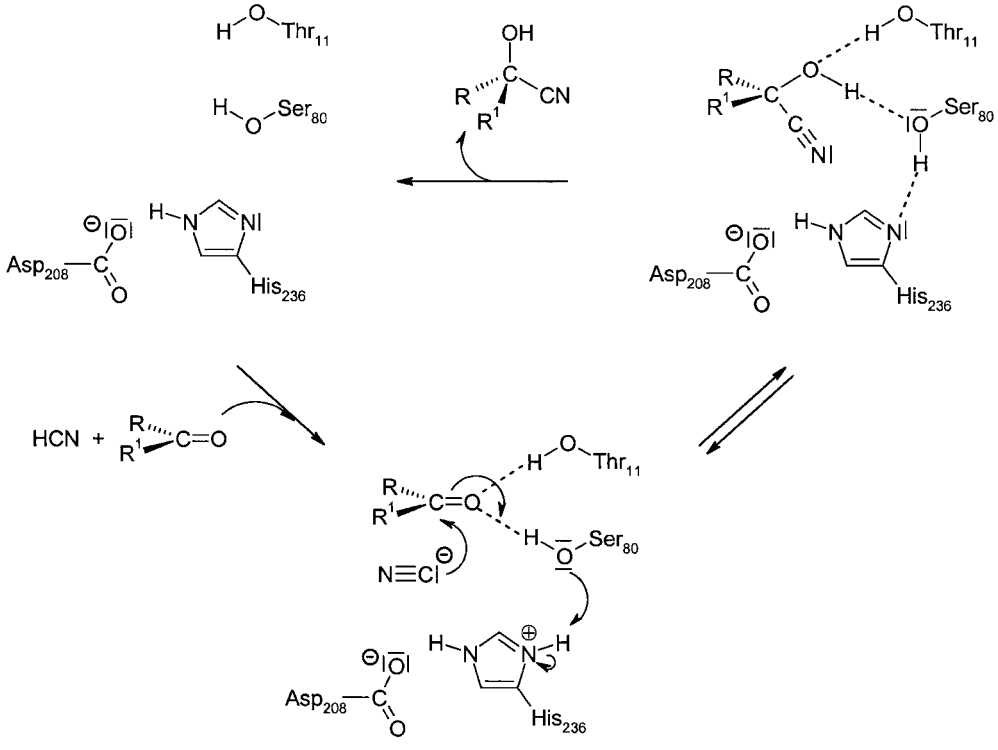

Figure 5
Catalytic mechanism of MeHNL. This mechanism is a modification of that proposed by Wajant & Pfizenmaier (1996) and is consistent with results discussed in the text.

We thank U. Schwaneberg for the fermentation of recombinant MeHNL. We also would like to thank the EMBL outstation at DESY, Hamburg for the use of data-collection facilities at beamline X11 and A. Baro for her help in preparing the manuscript as well as W. Saenger for critical reading of the manuscript. This work was generously supported by the EU project 'Hydroxynitrile Lyases for Industrial Enantioselective Synthesis' ERB BIO CT 960112, the Bundesministerium für Bildung und Forschung (Zentrales Schwerpunktprogramm Bioverfahrenstechnik B3.8U, Universität Stuttgart) and the Degussa-Hüls AG.

References

BIOSYM/Molecular Simulations Inc. (1995). *INSIGHT II/ DISCOVER* program, Release 95.0.

Brünger, A. T. (1992*a*). *X-PLOR. Version* 3.1. *A System for X-ray Crystallography and NMR.* Yale University, Connecticut, USA.

Brünger, A. T. (1992*b*). *Nature (London)*, **355**, 472–475.

Chueskul, S. & Chulavatnatol, M. (1996). *Arch. Biochem. Biophys.* **334**, 401–405.

Collaborative Computational Project, Number 4 (1994). *Acta Cryst.* D**50**, 760–763.

Effenberger, F. (1994). *Angew. Chem. Int. Ed. Engl.* **33**, 1555–1564.

Effenberger, F. (1999). *Chimia*, **53**, 3–10.

Förster, S., Roos, J., Effenberger, F., Wajant, H. & Sprauer, A. (1996). *Angew. Chem. Int. Ed. Engl.* **35**, 437–439.

Gerstner, E. & Pfeil, E. (1972). *Hoppe Seyler's Z. Physiol. Chem.* **353**, 271–286.

Griengl, H., Hickel, A., Johnson, D. V., Kratky, C., Schmidt, M. & Schwab, H. (1997). *J. Chem. Soc. Chem. Commun.*, pp. 1933–1940.

Hasslacher, M., Schall, M., Hayn, M., Griengl, H., Kohlein, S. D. & Schwab, H. (1996). *J. Biol. Chem.* **271**, 5884–5891.

Jones, T. A. (1978). *J. Appl. Cryst.* **11**, 268–272.

Lauble, H., Decanniere, K., Wajant, H., Förster, S. & Effenberger, F. (1999). *Acta Cryst.* D**55**, 904–906.

North, M. (1993). *Synlett*, pp. 807–820.

Otwinowski, Z. (1993). *DENZO: An Oscillation Data Processing Program for Macromolecular Crystallography*. Yale University, Connecticut, USA.

Schmidt, M., Hervé, S., Klempier, N. & Griengl, H. (1996). *Tetrahedron*, **52**, 7833–7840.

Seigler, D. S. (1991). *Herbivores: Their Interactions with Secondary Plant Metabolites*, edited by G. A. Rosenthal & M. R. Berenbaum, pp. 35–77. New York: Academic Press.

Trummler, K. & Wajant, H. (1997). *J. Biol. Chem.* **272**, 4770–4774.

Wagner, U. G., Hasslacher, M., Griengl, H., Schwab, H. & Kratky, C. (1996). *Structure*, **4**, 811–822.

Wajant, H. & Effenberger, F. (1996). *Biol. Chem.* **377**, 611–617.

Wajant, H. & Förster, S. (1996). *Plant Sci.* **115**, 25–31.

Wajant, H., Förster, S., Böttinger, H., Effenberger, F. & Pfizenmaier, K. (1995). *Plant Sci.* **108**, 1–11.

Wajant, H., Mundry, K.-W. & Pfizenmaier, K. (1994). *Plant Mol. Biol.* **26**, 735–746.

Wajant, H. & Pfizenmaier, K. (1996). *J. Biol. Chem.* **271**, 25830–25834.

Zuegg, J., Gruber, K., Gugganig, M., Wagner, U. G. & Kratky, C. (1999). *Protein Sci.* **8**, 1990–2000.